nature microbiology

SUPPLEMENTARY INFORMATION

https://doi.org/10.1038/s41564-018-0199-2

In the format provided by the authors and unedited.

Escherichia coli translation strategies differ across carbon, nitrogen and phosphorus limitation conditions

Sophia Hsin-Jung Li[1], Zhiyuan Li[2], Junyoung O. Park[3,4,7], Christopher G. King[5], Joshua D. Rabinowitz[3,6], Ned S. Wingreen[1,3]* and Zemer Gitai[1]*

[1]Department of Molecular Biology, Princeton University, Princeton, NJ, USA. [2]Princeton Center for Theoretical Science, Princeton University, Princeton, NJ, USA. [3]Lewis-Sigler Institute for Integrative Genomics, Princeton University, Princeton, NJ, USA. [4]Department of Chemical and Biological Engineering, Princeton University, Princeton, NJ, USA. [5]Department of Physics, Princeton University, Princeton, NJ, USA. [6]Department of Chemistry, Princeton University, Princeton, NJ, USA [7]Present address: Department of Chemical and Biomolecular Engineering, University of California, Los Angeles, CA, USA. *e-mail: wingreen@princeton.edu; zgitai@princeton.edu

Supplementary Information for

E. coli translation strategies differ across carbon, nitrogen, and phosphorus limitation conditions

Sophia Hsin-Jung Li, Zhiyuan Li, Junyoung O. Park, Christopher G. King, Joshua D. Rabinowitz, Ned S. Wingreen*, and Zemer Gitai*

*Correspondence to wingreen@princeton.edu, zgitai@princeton.edu

The supplementary information contains:

1. Comparison of RNA-to-protein ratio data with published results

Multiple groups have published the results of RNA-to-protein ratios in a variety of growth conditions, particularly in batch culture using various carbon and nitrogen sources [1-5]. We compared cells grown in our chemostat and batch culture conditions and found that the R/P ratios from batch cultures with different carbon and nitrogen sources overlapped with the R/P ratios from chemostat cultures under carbon and nitrogen limitation (Supplementary Fig. 1a). This result suggests that our findings are not chemostat-specific. We also confirmed that R/P ratio represents a good proxy for ribosome content using bioanalyzer analysis of total RNA. At all growth rates, rRNA fractions remained similar across C/N/P-limitation. We also found that rRNA fractions increased with increasing growth rate (Supplementary Fig. 1e), while tRNA fractions decreased with increasing growth rate (Supplementary Fig. 1f). These measurements showed a similar trend to previously published data regardless of the nutrient limitation [6-8]. Since P-limited cells have both the lowest R/P ratio and the lowest rRNA fraction, we concluded that under phosphorus limitation cells have lower ribosome content than under carbon or nitrogen limitation.

We also determined the R/P ratio of cells grown faster (1.2 h^{-1}) in P-limiting chemostats using defined rich media with reduced phosphate concentration. We found that even at fast growth, P-limited cells still exhibit lower R/P ratio compared to batch culture. This result implies that cells do not only maintain spare protein production capacity at very slow growth rates.

Comparing our results to published data from the same strain of *E.coli*, we noticed that there is a shift in the R/P ratio absolute values (Supplementary Fig. 1b). Because the change was consistent in all samples and our batch cultures of the same conditions also exhibited higher R/P ratio values, we reasoned this systematic shift might be due to differences in experimental setups, such as differences in the protein standard used.

2. Microscopic model of ribosome dynamics along an mRNA

Ribosome profiling provides positional information of ribosomes occupancy on mRNA transcripts at single nucleotide resolution. In order to investigate ribosomal dynamics on transcripts, we built a microscopic model to estimate the position-dependent behavior of mRNA-bound ribosomes. As shown in the following part of this section, the modeling results lead to a classification of mRNA-bound ribosomes into two groups: “initiating” and “working”, which helps us to build a concise macroscopic model in Section 3.

A. Construction of a representative ribosome-occupancy profile.

We first combine the experimentally obtained ribosome profiling data to obtain an average picture for ribosome occupancy along a “representative” gene with length $N_{\mathrm{aa}} = 300$ amino acids [9]. The average ribosome occupancy $O(x)$ for codon position $x = 1{:}\,301$, including the stop codon, was constructed via the following steps:

1. All genes that code for proteins longer than 100 aa and have counts larger than 10 transcripts per million (TPM) were selected. This set of genes accounts for more than 75% of total reads.
2. Total counts from the selected genes were normalized to one million (yielding reads per million, RPM) and the ribosome counts at the first and last 50 codons were obtained by summing the RPM at the corresponding position from all the selected genes (result shown in Fig. 2a and Supplementary Fig. 5c) and converted to fraction of total counts. This procedure effectively weights genes in the representative ribosome-count profile according to their level of expression.
3. We used the data from the first 50 codons and the last 49 codons before the stop codon to produce a smooth fit to the experimentally obtained ribosome-count profile. A gap with length 201 was inserted between the first 50 and last 49 codons before the stop codon to produce an mRNA producing 300 amino acids. In order to capture the sharp drop of ribosome counts for the first several codons, together with the slower decrease over the rest of the profile, we used a sum of two decaying exponential functions to fit the data. The experimentally measured ribosome count from the stop codon ($x = 301$) was directly taken from the data without fitting. The final results are shown in Supplementary Fig. 5c.

B. The microscopic model for bound ribosomes.

In order to decipher the information about ribosome dynamics contained in ribosome occupancy $O(x)$, we built a microscopic model shown in Supplementary Fig. 5b. In this simplified model, bound ribosomes on codon x move with a step rate $r_s(x)$, and a certain fraction $f_{at}(x)$ abort translation during this transition. At steady state, the in- and out-flux of ribosomes at every codon *x* must be balanced:

$$O(x-1)\cdot r_s(x-1)\cdot\big(1-f_{at}(x-1)\big) = O(x)\cdot r_s(x). \qquad \textbf{Eq.S 1}$$

According to Eq.S 1, under steady state, the relative occupancy of neighboring codons is determined by the step rate and fraction of aborted translation. The profile of $O(x)$ constrains the values of $r_s(x)$ and $f_{at}(x)$. We would like to infer the value of $r_s(x)$ and $f_{at}(x)$ given $O(x)$ within some assumptions. Two possibilities concerning the profile of $O(x)$ and the corresponding assumptions are listed below:

1. *O*(*x*) decreases with x. This implies an increased step rate r_s and/or a non-zero fraction of aborted translation f_{at}. For simplicity, we assume a constant fraction (f_{dec}) of the decrease of occupancy ($\frac{O(x-1)}{O(x)}-1$) can be attributed to an increased step rate ($\frac{r_s(x)}{r_s(x-1)}-1$):

$$f_{\mathrm{dec}} = \frac{\frac{r_{\mathrm{s}}(x)}{r_{\mathrm{s}}(x-1)} - 1}{\frac{O(x-1)}{O(x)} - 1}. \qquad \textbf{Eq.S 2}$$

2. $O(x)$ does not decrease with x. This implies that the step rate r_{s} does not increase with x. Under this condition, the higher f_{at}, the more r_{s} decreases with x. According to previous research, the translation elongation rate of ribosomes generally increases from 5' to 3'[10, 11]. Therefore, we assume $f_{\mathrm{at}} = 0$ under this condition.

With the former assumptions, we can derive $r_{\mathrm{s}}(x-1)$ and $f_{\mathrm{at}}(x-1)$ given $r_{\mathrm{s}}(x)$:

$$r_{\mathrm{s}}(x-1) = \begin{cases} \dfrac{r_{\mathrm{s}}(x)}{f_{\mathrm{dec}} \cdot \left(\dfrac{O(x-1)}{O(x)} - 1\right) + 1}, & \text{if } \dfrac{O(x-1)}{O(x)} > 1 \\ r_{\mathrm{s}}(x) \cdot \dfrac{O(x)}{O(x-1)}, & \text{if } \dfrac{O(x-1)}{O(x)} \leq 1 \end{cases}, \qquad \textbf{Eq.S 3}$$

$$f_{\mathrm{at}}(x-1) = \begin{cases} (1 - f_{\mathrm{dec}}) \cdot \left(1 - \dfrac{O(x)}{O(x-1)}\right), & \text{if } \dfrac{O(x-1)}{O(x)} > 1 \\ 0, & \text{if } \dfrac{O(x-1)}{O(x)} \leq 1 \end{cases}. \qquad \textbf{Eq.S 4}$$

C. Calculation of step rate $r_{\mathrm{s}}(x)$ and fraction of aborted translation $f_{\mathrm{at}}(x)$.

By applying Eq.S 3 - Eq.S 4 to the ribosome occupancy $O(x)$ obtained experimentally in Section 2A, we can calculate r_{s} and f_{at} from $x = 300$ to $x = 1$, for assumed values of f_{dec} and the step rate at the last coding codon $r_{\mathrm{s}}(300)$. The existence of aborted translation has been suggested by previous studies [10, 12], however the quantitative fraction of aborted translation under different nutrient-limitations is difficult to quantify. Given the uncertainty of the aborted translation rate, we evenly sampled values of f_{dec} from 0 to 1 and values of $r_{\mathrm{s}}(300)$ from 5 to 20 codon/sec. Each combination of f_{dec} and $r_{\mathrm{s}}(300)$ gives a solution for $r_{\mathrm{s}}(x)$ and $f_{\mathrm{at}}(x)$ from $x = 300$ to $x = 1$. The results are shown in Supplementary Fig. 5d-e: regardless of f_{dec} and $r_{\mathrm{s}}(300)$, aborted translation predominantly happens within the first 10 codons, and the step rate stays relatively flat after the first 10 codons.

D. Classification of ribosomes and mRNAs.

Guided by the above results, we classify mRNA-bound ribosomes into two groups:

1. Initiating ribosomes (symbolized by R_{i}): ribosomes located within codon 1 to 10 are classified as "initiating". Given the results in Section 2C, we assume that aborted translation, if it exists at all, only happens to this group of ribosomes. As one ribosome roughly occupies 10 codons on an mRNA [13, 14], the binding

of one ribosome at the initiating region excludes the association of another ribosome. Thereby mRNAs are divided into two groups: the freely initiable mRNAs (symbolized by M_{f}), and the un-initiable mRNAs with one ribosome occupying the 1-10 codon region (symbolized by M_{b}). By definition, the number of un-initiable mRNAs is equal to the number of initiating ribosomes.

2. Working ribosomes (symbolized by R_{w}): ribosomes located after the 10-th codon are classified as "working". They contribute to the increase of biomass. We assume that these ribosomes elongate at a constant rate k_{el} without terminating translation prematurely. Under this assumption, there is no aborted translation in transition from the last coding codon ($x = 300$) to the stop codon ($x = 301$), and the number of ribosomes transiting from the last coding codon to the stop codon is equal to the number of ribosomes leaving stop codon in a steady state. Therefore, the ribosome occupancy at stop codon does not influence the overall protein production rate. In addition, ribosome occupancies at the stop codon are similar across different nutrient-limitations (Fig. 2a), and only take about 2% of total ribosomes. Therefore, we count ribosomes at stop codon also as "working ribosomes" instead of classifying them into another group.

3. Macroscopic model of ribosome dynamics among different states

A. Dynamics of ribosomes and mRNAs between different states.

In Section 2, we classified the mRNA-bound ribosomes into "initiating" and "working" states. This result allowed us to construct a macroscopic model that provides a concise picture of ribosomal dynamics. The transition of ribosomes between three states is shown in Fig. 2b. As ribosomal subunits and free 70S ribosomes may convert between each other, they are treated as one group, named unbound ribosomes (symbolized by R_{u}). A sub-population of the unbound ribosomes can associate with freely initiable mRNAs (M_{f}) with an effective rate constant k_{f}. This reaction forms a complex composed of an initiating ribosome (R_{i}) and an un-initiable mRNA (M_{b}). The initiating ribosomes either become unbound ribosomes through aborted translation (with rate constant k_{r}), or proceed to the 11-th codon to become working ribosomes (R_{w}) (with rate constant k_{p}). Both processes can release the mRNA back to the freely initiable state. The working ribosomes elongate with constant rate k_{el}. At the last coding codon, a fraction of bound ribosomes ($\sim 1/N_{\mathrm{aa}}$) enters stop codon with rate k_{el}, and the same number of ribosomes completes translation and releases mRNA and become unbound ribosomes.

The non-redundant kinetic ordinary differential equations for the number of ribosomes and mRNAs in each state are:

$$\frac{dR_{\mathrm{i}}}{dt} = k_{\mathrm{f}} \cdot M_{\mathrm{f}} \cdot R_{\mathrm{u}} - k_{\mathrm{r}} \cdot R_{\mathrm{i}} - k_{\mathrm{p}} \cdot R_{\mathrm{i}}, \quad \textbf{Eq.S 5}$$

$$\frac{dR_{\mathrm{w}}}{dt} = k_{\mathrm{p}} \cdot R_{\mathrm{i}} - \frac{k_{\mathrm{el}}}{N_{\mathrm{aa}}} \cdot R_{\mathrm{w}}, \quad \textbf{Eq.S 6}$$

$$\frac{dM_{\mathrm{f}}}{dt} = -k_{\mathrm{f}} \cdot M_{\mathrm{f}} \cdot R_{\mathrm{u}} + k_{\mathrm{p}} \cdot R_{\mathrm{i}} + k_{\mathrm{r}} \cdot R_{\mathrm{i}}. \quad \textbf{Eq.S 7}$$

Under steady-state growth conditions, the fluxes between ribosomal states should be balanced, and the right-hand sides of Eq.S 5 - Eq.S 7 should all be equal to zero (the production and degradation/dilution by growth of new ribosomes and mRNAs occurs at a negligible rate compared to their recycling). The total number of ribosomes (R_t) and the total number of mRNAs (M_t) are constant parameters for this model:

$$R_\mathrm{u} + R_\mathrm{i} + R_\mathrm{w} = R_\mathrm{t}, \quad \textbf{Eq.S 8}$$

$$M_\mathrm{b} + M_\mathrm{f} = M_\mathrm{t}, \quad \textbf{Eq.S 9}$$

and by the definition in Section 2D,

$$M_\mathrm{b} = R_\mathrm{i}. \quad \textbf{Eq.S 10}$$

B. Estimation of R_t, M_t, k_el, and k_p from experimental measurements.

We are interested in the biological mechanisms that lead to distinct ribosomal dynamics under different nutrient conditions. Possible regulatory processes can be represented by parameters in the macroscopic model, including the total number of ribosomes and mRNAs and the rates for ribosomes to initiate, dissociate, and elongate. Some of these parameters, specifically R_t , M_t, k_el, and k_p, can be directly estimated from experimental measurements as follows:

1. The total number of ribosomes (R_t): The total mass of rRNA can be obtained by multiplying the RNA-to-protein ratio (RPR), protein mass in a cell (P_m), and the fraction of RNA as rRNA (f_r). Given the mass of the rRNA in a ribosome as m_r, we estimated the total number of ribosomes in a cell:

$$R_\mathrm{t} = P_\mathrm{m} \cdot RPR \cdot \frac{f_\mathrm{r}}{m_\mathrm{r}}. \quad \textbf{Eq.S 11}$$

2. The total number of mRNAs in a cell (M_t): The method is similar to the calculation of R_t in Eq.S 11. Given the fraction of RNA as mRNA as f_m, and the average weight of a nucleotide as m_nuc, we have:

$$M_t = P_\mathrm{m} \cdot RPR \cdot \frac{f_\mathrm{m}}{N_\mathrm{aa} \cdot m_\mathrm{nuc} \cdot 3}. \quad \textbf{Eq.S 12}$$

3. The protein synthesis rate (J_P): The amount of newly synthesized proteins in a cell per second is defined as J_P (aa/sec). J_P can be calculated by two ways: One, the growth rate μ (h^{-1}) can be calculated as the relative rate of protein mass accumulation: $\mu = \frac{J_\mathrm{P}}{P_\mathrm{m}/m_\mathrm{aa}}$, where m_aa is the average mass of amino acid (g). Therefore, J_P is linearly proportional to the growth rate:

$$J_{\mathrm{P}} = \mu \cdot \left(\frac{P_{\mathrm{m}}}{3600 \cdot m_{\mathrm{aa}}}\right). \qquad \textbf{Eq.S 13}$$

J_{P} can also be calculated from the contribution of working ribosomes to the growth of the total protein pool:

$$J_{\mathrm{P}} = R_{\mathrm{w}} \cdot k_{\mathrm{el}}\,. \qquad \textbf{Eq.S 14}$$

Combining Eq.S 13 and Eq.S 14, the growth rate μ is determined by three factors: the total number of ribosomes (R_{t}), the fraction of working ribosomes ($\emptyset_{\mathrm{Rw}}$), and the average elongation rate of the working ribosomes (k_{el}):

$$\mu = R_{\mathrm{t}} \cdot \emptyset_{\mathrm{Rw}} \cdot k_{\mathrm{el}} \cdot \left(\frac{3600 \cdot m_{\mathrm{aa}}}{P_{\mathrm{m}}}\right). \qquad \textbf{Eq.S 15}$$

The contribution of these three factors to the growth rate is illustrated by Table 1. The surface in the space of these three factors that corresponds to growth rate $\mu = 0.1\ \mathrm{h}^{-1}$ is shown in Fig. 2e and Supplementary Fig. 6f, with the estimated values of R_{t}, $\emptyset_{\mathrm{Rw}}$, and k_{el} under various conditions indicated on this surface.

Substituting R_{t} in Eq.S 15 by Eq.S 11, the relationship between the four experimentally measured values – growth rate (μ), RNA-to-protein ratio (RPR), average elongation rate (k_{el}), and fraction of working ribosomes ($\emptyset_{\mathrm{Rw}}$) – is given by:

$$\mu = RPR \cdot \emptyset_{\mathrm{Rw}} \cdot k_{\mathrm{el}} \cdot \left(3600 \cdot m_{\mathrm{aa}} \cdot \frac{f_{\mathrm{r}}}{m_{\mathrm{r}}}\right). \qquad \textbf{Eq.S 16}$$

Eq.S 16 can be used to estimate growth rate as shown in Table 1. Using different definitions of $\emptyset_{\mathrm{Rw}}$, we show that it can lead to different estimations of growth rate. The $\emptyset_{\mathrm{Rw}}$ we used for modeling is from the following Section 3B4. While growth rate, RNA-to-protein ratio and fraction of working ribosomes are global measurements, the elongation rate was measured using the *lacZ* induction assay. For the rRNA fraction (f_{r}) we used the experimentally measured values from Supplementary Fig. 1e.

In order to obtain a global estimate of the elongation rate k_{el}, we derived k_{el} from the measurements of growth rate, RNA-to-protein ratio, and the fraction of working ribosomes by the following steps 4-5.

4. Quantifying the fraction of different ribosomal species: The fraction of unbound ribosomes is the sum of the free 70S fraction and the subunit fraction ($\emptyset_{\mathrm{Ru}} = \emptyset_{\mathrm{R70Sf}} + \emptyset_{\mathrm{Rs}}$). The fraction of initiating ribosome is

calculated by multiplying the fraction of bound ribosomes by the sum of ribosome occupancies at the first 10 codon ($\emptyset_{\mathrm{Ri}} = \sum_{x=1}^{10} O(x) \cdot (\emptyset_{\mathrm{R70Sb}} + \emptyset_{\mathrm{Rpoly}})$). The fraction of working ribosomes is calculated by multiplying the fraction of bound ribosomes with the summation of ribosome occupancy at the 11-th to 301-th codon ($\emptyset_{\mathrm{i}} = \sum_{\mathrm{x}=11}^{301} O(x) \cdot (\emptyset_{\mathrm{R70Sb}} + \emptyset_{\mathrm{Rpoly}})$).

5. Estimating the average working ribosome elongation rate k_{el}: From Eq.S 16 and the definition of $\emptyset_{\mathrm{Rw}}$, k_{el} can be calculated by measurements of *RPR* and $\emptyset_{\mathrm{Rw}}$:

$$k_{\mathrm{el}} = \frac{\mu}{RPR \cdot \emptyset_{\mathrm{Rw}} \cdot 3600 \cdot m_{\mathrm{aa}} \cdot \frac{f_{\mathrm{r}}}{m_{\mathrm{r}}}}. \qquad \textbf{Eq.S 17}$$

The resulting k_{el} is within the error range of the elongation rates measured from the *lacZ* induction assay (Supplementary Fig. 6a).

6. The rate constant k_{p} for ribosomes to proceed from initiating to working: According to Eq.S 6, at steady state,

$$k_{\mathrm{p}} = \frac{k_{\mathrm{el}}}{N_{\mathrm{aa}}} \cdot \frac{\emptyset_{\mathrm{Rw}}}{\emptyset_{\mathrm{Ri}}}. \qquad \textbf{Eq.S 18}$$

C. Fraction of working ribosomes ($\emptyset_{\mathrm{Rw}}$) as a function of kinetic parameters.

Among the three factors in Eq.S 15 that determine growth rate, R_{t} and k_{el} are parameters of the macroscopic model. In contrast, the fraction of working ribosomes, $\emptyset_{\mathrm{Rw}}$, is the outcome of dynamic processes described by the parameters in the macroscopic model. We would like to infer the relationship between $\emptyset_{\mathrm{Rw}}$ and these parameters, in order to identify the mechanisms that lead to the different observed $\emptyset_{\mathrm{Rw}}$ under different conditions.

The parameters k_{r} and k_{f} cannot be obtained experimentally. Nevertheless, we will show in the following part of this section that these two parameters work in combination to influence the value of $\emptyset_{\mathrm{Rw}}$, and the combined parameter can be obtained from experimental measurements.

According to Eq.S 5-Eq.S 10, in steady state, we obtained an expression for $\emptyset_{\mathrm{Rw}}$:

$$\emptyset_{\mathrm{Rw}} = \frac{F}{2} \cdot \left(\left(\frac{1}{S \cdot (F+1)} + \frac{M_{\mathrm{t}}}{R_{\mathrm{t}}} \right) - \left(\left(\frac{1}{S \cdot (F+1)} + \frac{M_{\mathrm{t}}}{R_{\mathrm{t}}} \right)^2 - 4 \cdot \frac{M_{\mathrm{t}}}{R_{\mathrm{t}}} \cdot \frac{1}{F+1} \right)^{\frac{1}{2}} \right), \qquad \textbf{Eq.S 19}$$

with

$$F = N_{\mathrm{aa}} \cdot \frac{k_{\mathrm{p}}}{k_{\mathrm{el}}},$$

$$K_{\mathrm{M}} = \frac{k_{\mathrm{r}} + k_{\mathrm{p}}}{k_{\mathrm{f}}},$$
$$S = \frac{R_{\mathrm{t}}}{K_{\mathrm{M}} + R_{\mathrm{t}}}.$$

Eq.S 19 depends on three combined parameters: $\frac{M_{\mathrm{t}}}{R_{\mathrm{t}}}$ and F, S. According to Eq.S 11 and Eq.S 12, $\frac{M_{\mathrm{t}}}{R_{\mathrm{t}}} = \frac{f_{\mathrm{m}} \cdot m_{\mathrm{r}}}{N_{\mathrm{aa}} \cdot m_{\mathrm{nuc}} \cdot 3 \cdot f_{\mathrm{r}}}$ is a constant across different conditions under our assumptions. Physically, the combined parameter F can be interpreted as the "relative proceeding rate", reflecting the rate for ribosomes to proceed from an initiating to a working state relative to the average elongation rate. If there were no regulation at this step, F would be constant across different conditions regardless of elongation rates. However, if there is nutrient-specific regulation on the step rate or aborted translation rate within the first 10 codons, F will have different values for different conditions. The value of F can be calculated from the ribosomal profiling data according to Eq.S 18: $F = \frac{\sum_{x=11}^{x=301} O(x)}{\sum_{x=1}^{x=10} O(x)}$. Supplementary Fig. 6b shows the values of F under C-, N-, P-limitations ($\mu = 0.1\ \mathrm{h}^{-1}$) and Minimal condition ($\mu = 0.9\ \mathrm{h}^{-1}$) for WT and the *relA* mutant.

The lumped parameter S can be interpreted as a "saturation parameter": According to Eq.S 5-Eq.S 10 and Eq.S 13-Eq.S 14, the growth rate can be expressed as a function of R_{u}, mimicking the form of Michaelis-Menten:

$$\mu(R_{\mathrm{u}}) = \frac{3600 \cdot N_{\mathrm{aa}} \cdot m_{\mathrm{aa}}}{P_{\mathrm{m}}} \cdot M_{\mathrm{t}} \cdot k_{\mathrm{p}} \cdot \frac{R_{\mathrm{u}}}{K_{\mathrm{m}} + R_{\mathrm{u}}}. \qquad \textbf{Eq.S 20}$$

In analogy to enzymatic reactions, in our model, ribosome subunits can be viewed as the substrates, mRNA as the enzyme, and working ribosomes as the product, and therefore K_{m} is interpreted as the half-saturation concentration of unbound ribosomes. Therefore, $S = \frac{R_{\mathrm{t}}}{K_{\mathrm{m}} + R_{\mathrm{t}}}$ positively correlates with the degree of saturation for ribosomes in translation: A value of S near zero implies a large fraction of mRNAs are initiable, waiting for ribosomes, while S approaching one implies most mRNAs are occupied in the initiation region and increasing in ribosome number cannot substantially boost growth rate. The value of S can be calculated by quantifying the ribosomal species according to Eq.S 5, Eq.S 11, and Eq.S 12: $S = 1/(1 + (\frac{f_{\mathrm{m}} \cdot m_{\mathrm{r}}}{N_{\mathrm{aa}} \cdot m_{\mathrm{nuc}} \cdot 3 \cdot f_{\mathrm{r}}} - \phi_{\mathrm{Ri}}) \cdot \frac{\phi_{\mathrm{Ru}}}{\phi_{\mathrm{Ri}}})$. Supplementary Fig. 6c shows the values of S under C-, N-, P-limitations ($\mu = 0.1\ \mathrm{h}^{-1}$) and Minimal condition ($\mu = 0.9\ \mathrm{h}^{-1}$) for wild type and the *relA* mutant.

According to Eq.S 19, $\emptyset_{\mathrm{Rw}}$ is an increasing function of both F and S. In wild type, the relative proceeding rate F and the saturation parameter S both increase from C-, N- P-limitation to Minimal condition, leading to an increasing $\emptyset_{\mathrm{Rw}}$. The *relA* mutant under P-limitation has a very high relative proceeding rate,

consistent with the known biological role of *relA*. By contrast, the loss of *relA* does not affect the saturation parameter.

D. Growth rate μ as a function of total ribosome number R_t and total mRNA number M_t.

Given our detailed estimation of the parameters associated with translation under different nutrient conditions, we are interested in how the total number of ribosomes may influence the protein production rate, and whether ribosome number is the limiting factor for cell growth.

Combining Eq.S 15 and Eq.S 19, yields the growth rate μ as a function of R_t, and other kinetic parameters of the macroscopic model:

$$\mu(R_t) = \left(\frac{3600 * m_{aa}}{P_m}\right) \cdot \frac{k_p}{2} \cdot N_{aa} \cdot \left((A \cdot K_M + A \cdot R_t + M_t) - ((A \cdot K_M + A \cdot R_t + M_t)^2 - 4 \cdot M_t \cdot R_t \cdot A)^{\frac{1}{2}} \right), \quad \textbf{Eq.S 21}$$

with

$$A = \frac{1}{F+1} = \frac{1}{\frac{N_{aa} \cdot k_p}{k_{el}} + 1}.$$

This function resembles the shape of a Michaelis-Menten function of both R_t and M_t. Intuitively, μ = 0 when R_t or M_t equal to zero. If R_t increases while M_t is held constant, μ monotonically increases and saturates at

$$\mu(\infty) = \left(\frac{3600 \cdot m_{aa}}{P_m}\right) * k_p * N_{aa} * M_t. \quad \textbf{Eq.S 22}$$

The half-saturation value of R_t is also linearly increasing with M_t:

$$R_{t,1/2} = \frac{1}{2 \cdot A} \cdot M_t + K_M. \quad \textbf{Eq.S 23}$$

Supplementary Fig. 6d-e show the functions $\mu(R_t)$ and the estimated values of R_t under different nutrient conditions while M_t is held constant.

As shown in Supplementary Fig. 6d-e, in all conditions, the estimated numbers of ribosomes are much smaller than the half-saturation value, falling into the highly linear region, It supports that ribosomes are the limiting factors for cell growth. In future, it will be interesting to directly probe the degree of saturation for ribosomes experimentally.

E. Predicting the growth rate after nutrient upshift to rich medium.

As mentioned in the main text, there appear to be diverse strategies that achieve the same growth rate under different nutrient limitations, but these strategies may lead to different outcomes when the environment changes. One possibility is that having extra ribosomes at slow growth rates can enable a faster recovery when nutrients become abundant again. Therefore, we expanded our

macroscopic model beyond steady state to predict growth dynamics upon nutrient upshift.

The rate of cell growth positively correlates with the rate of protein synthesis. Among newly synthesized proteins, a certain fraction of mass is allocated to ribosomal proteins ($\Psi_{\mathrm{R}}(t)$). The steady-state value of this mass fraction (Ψ_{R}^{*}) under a given condition (i) can be calculated from the estimated number of total ribosomes:

$$\Psi_{\mathrm{R,i}}^{*} = R_{\mathrm{t}} \cdot N_{\mathrm{Raa}} \cdot \frac{m_{\mathrm{aa}}}{P_{\mathrm{m}}}. \qquad \textbf{Eq.S 24}$$

N_{Raa} is the number of amino acids in a ribosome, and m_{aa} is the average mass of an amino acid in *E. coli* protein. The time-dependent growth rate $g(t)$ of a bacterial population can be defined in terms of the increase in total cell volume:

$$g(t) = \frac{V'(t)}{V(t)}. \qquad \textbf{Eq.S 25}$$

Assuming the concentration of protein (C_{p}) remains constant, the rate of increase of total volume will be linearly related to the rate of increase of protein mass, which is proportional to the concentration of working ribosomes $r_{\mathrm{b}}(t)$ and the translation completion rate $k_{\mathrm{el}}/N_{\mathrm{aa}}$:

$$V'(t) = V(t) \cdot k_{\mathrm{el}} \cdot r_{\mathrm{b}}(t) \cdot \frac{m_{\mathrm{aa}}}{C_{\mathrm{p}}}. \qquad \textbf{Eq.S 26}$$

Based on Eq.S 25 and Eq.S 26, the growth rate can be expressed as:

$$g(t) = k_{\mathrm{el}} \cdot r_{\mathrm{b}}(t) \cdot \frac{m_{\mathrm{aa}}}{C_{\mathrm{p}}}. \qquad \textbf{Eq.S 27}$$

However, during the process of reaching steady state, $\Phi_{\mathrm{R}}(t)$ might be regulated, e.g. to accelerate cell growth, and therefore could be a time-dependent function.

Applying the chain rule of differentiation to intracellular concentrations, $\frac{d\left(\frac{X}{V}\right)}{dt} = \frac{1}{V} \cdot \frac{dX}{dt} - \frac{X}{V} \cdot \left(\frac{1}{V} \cdot \frac{dV}{dt}\right)$, the rates of change in the concentration of different ribosome species can be expressed as:

$$\frac{dr_{\mathrm{t}}(t)}{dt} = \Psi_{\mathrm{R}}(t) \cdot \frac{k_{\mathrm{el}}}{N_{\mathrm{aa}}} \cdot r_{\mathrm{w}}(t) - g(t) \cdot r_{\mathrm{t}}(t), \qquad \textbf{Eq.S 28}$$

$$\frac{dr_{\mathrm{i}}}{dt} = k_{\mathrm{f}} \cdot M_{\mathrm{f}} \cdot \left(r_t(t) - r_{\mathrm{i}}(t) - r_w(t)\right) - k_{\mathrm{r}} \cdot r_{\mathrm{i}}(t) - k_{\mathrm{p}} \cdot r_{\mathrm{i}}(t) - g(t) \cdot r_{\mathrm{i}}(t), \qquad \textbf{Eq.S 29}$$

$$\frac{dr_{\mathrm{w}}(t)}{dt} = k_{\mathrm{p}} \cdot r_{\mathrm{i}}(t) - \frac{k_{\mathrm{el}}}{N_{\mathrm{aa}}} \cdot r_{\mathrm{w}}(t) - g(t) \cdot r_{\mathrm{w}}(t). \qquad \textbf{Eq.S 30}$$

We are interested in the growth dynamics after switching cells from C-, N-, or P-limitation to rich medium. We therefore solved Eq.S 28-Eq.S 30 for parameter values obtained under rich condition. The initial states of r_{t}, r_{i}, and r_{w} were taken as their steady-state values (r_{t}^*, r_{i}^*, and r_{w}^*) under C-, N-, and P-limitations, respectively.

The fraction of newly synthesized ribosomal proteins $\Psi_{\mathrm{R}}(t)$ reflects the regulation of protein allocation by the cell. Eventually this value needs to reach the steady-state value Ψ_{R}^* in rich media. Nevertheless, during the transition period, different strategies of regulating $\Psi_{\mathrm{R}}(t)$ yield different growth dynamics. In our model, we tested three different control strategies for $\Psi_{\mathrm{R}}(t)$: Bang-Bang control

$$\left(\Psi_{\mathrm{R}}(t) = \begin{cases} 1 \ \left(\text{if } r_t < r_{\mathrm{t,rich}}^*\right) \\ \Psi_{\mathrm{R,rich}}^* \left(\text{if } r_t = r_{\mathrm{t,rich}}^*\right) \\ 0 \ \left(\text{if } r_t > r_{\mathrm{t,rich}}^*\right) \end{cases}\right), \qquad \textbf{Eq.S 31}$$

smooth control ($\Psi_{\mathrm{R}}(t) = 2 \cdot \Psi_{\mathrm{R,rich}}^* / (\frac{r_{\mathrm{t}}}{r_{\mathrm{t,rich}}^*} + 1)$), and steady-state control ($\Psi_{\mathrm{R}}(t)$= $\Psi_{\mathrm{R,rich}}^*$). “Bang-bang control” has been discovered in multiple domains of biology, and it has been shown that Bang-Bang control of regulation can maximize the accumulated increase of cell volume [7-9]. In our model, the control mechanism in Eq. S 33 allocates all resources into synthesis of ribosomes if the ribosome concentration is less than $r_{\mathrm{t,rich}}^*$, and shuts off the ribosomal protein production if the cellular concentration of ribosomes exceeds $\Psi_{\mathrm{R,rich}}^*$. Interestingly, we found that a Bang-Bang control strategy gave the prediction closest to our experimentally observed dynamics for nutrient-upshift (Supplementary Fig. 9). The other two possible mechanisms give rise to qualitatively similar dynamics for nutrient-upshift, where the C/N-limited cells recovers faster than P-limited cells in Rich condition; however, the predicted cell growth curves are slower than the experimental observation.

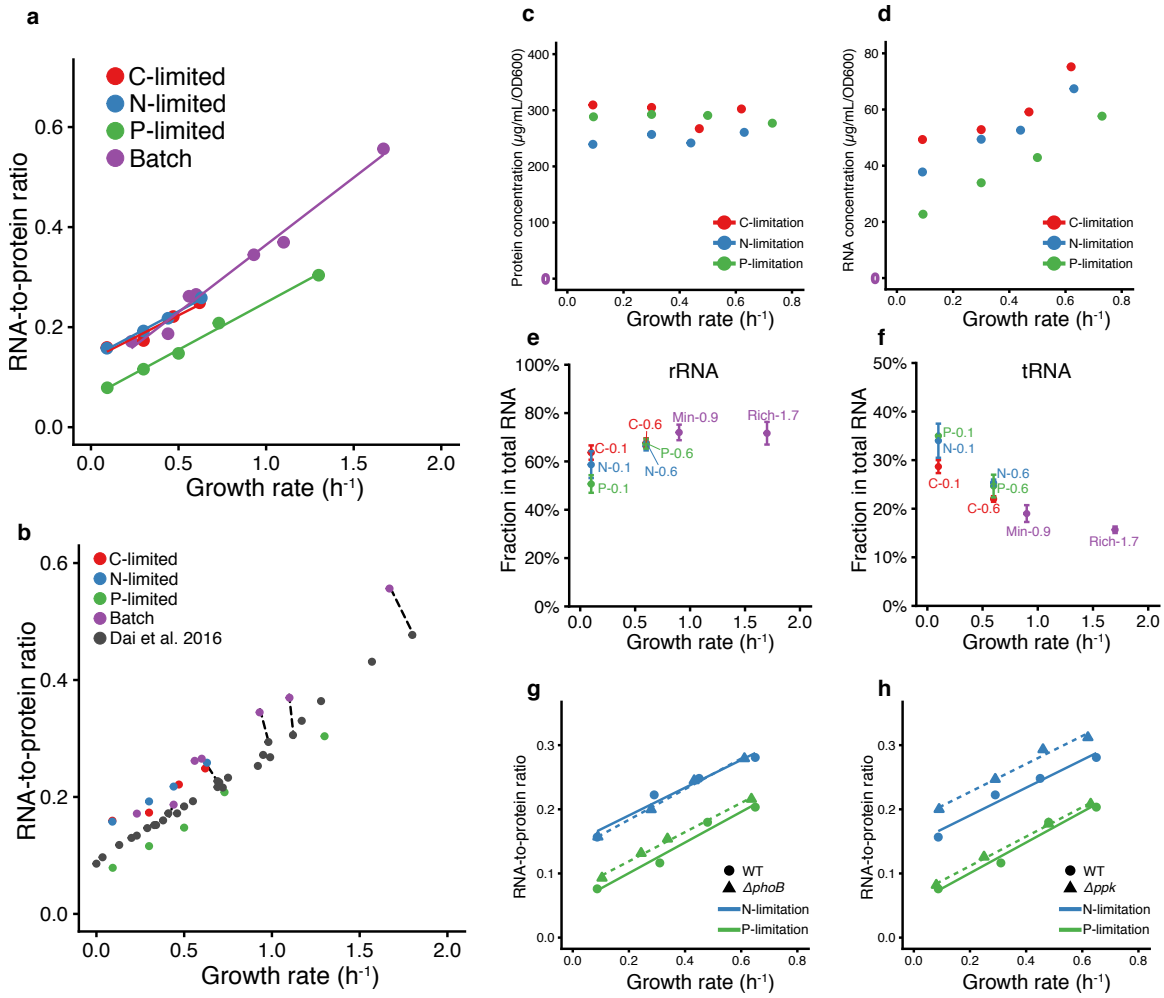

Supplementary Figure 1. (Related to Figure 1) Lower RNA-to-protein ratio under P-limitation results from lower RNA concentration, and phosphorus metabolism-related genes are not involved in the regulation. (a) RNA-to-protein ratio in chemostat and batch conditions. Each data point shows the mean value from three technical replicates. **(b)** Comparison of RNA-to-protein ratio values between this study and previously reported values from the same strain of *E. coli* NCM3722. Same conditions are connected by the dotted line. **(c)** Total protein (μg/mL/OD600) and **(d)** RNA (μg/mL/OD600) concentrations were measured. These data were used to generate Fig. 1b of the RNA-to-protein ratio. Each data point represents the mean value from three technical replicates. **(e-f)** Fraction of rRNA (e) and tRNA (f) in total RNA determined from bioanalyzer assay across different nutrient limitations and growth rates. Each data point shows the mean value from three biological replicates with error bars as SEM. **(g-h)** RNA-to-protein ratio for chemostat cultures of wild-type and mutant cells upon N-, and P-limitations at different growth rates. Each data point shows the mean value from three technical replicates: (g) *Δ phoB*, (h) *Δ ppk.*

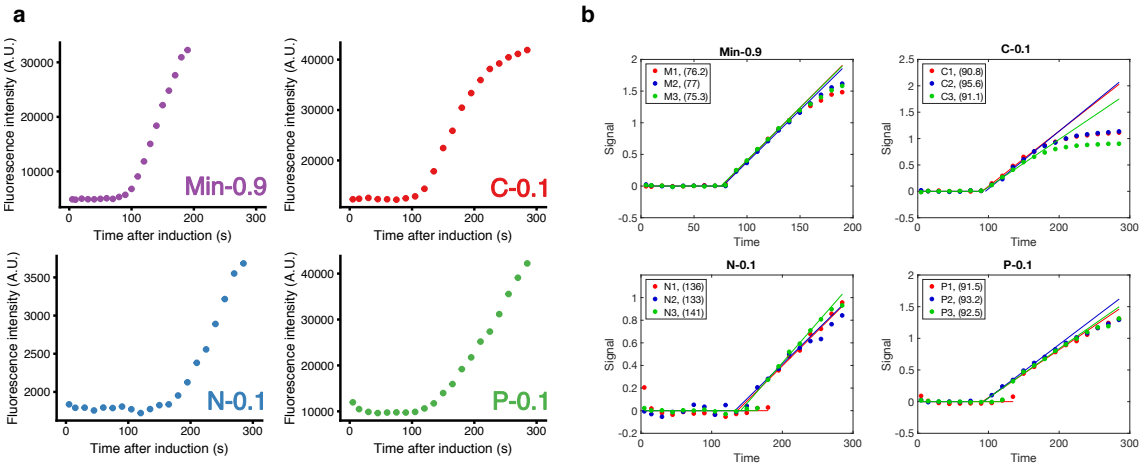

Supplementary Figure 2. (Related to Figure 1) *lacZ* induction curves and fittings for translational elongation rate measurements. (a) Raw data of *lacZ* induction time course for batch glucose minimal media (Min-0.9), C-, N-, and P-limited cells grown at 0.1 h^{-1}. Three biological replicates were performed and data from one representative replicate is shown for clarity. **(b)** Transformed *lacZ* induction data for lag time estimation. All three biological replicates are shown with estimated lag time indicated in the bracket (See Methods for detail).

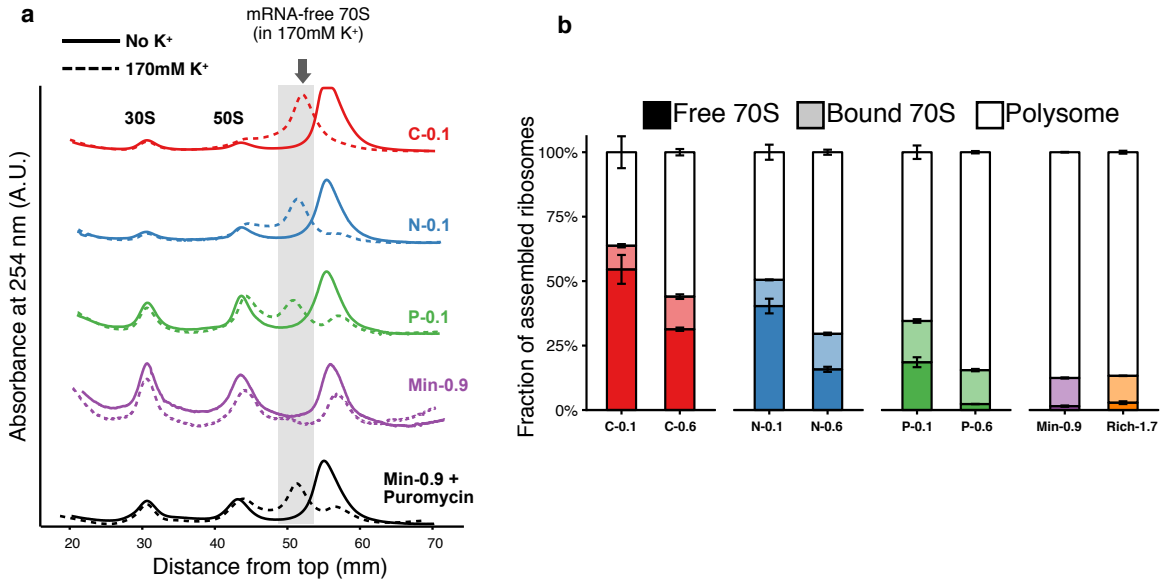

Supplementary Figure 3. (Related to Figure 1) Elevated [K^+] distinguishes mRNA-free from mRNA-bound 70S ribosomes. (a) The plot shows the separation of these two distinct 70S species under different growth conditions using 170 mM K^+. The A254 values are vertically shifted for each condition for easier visualization. Puromycin is used as a positive control for free ribosome accumulation and fast-growing cells in glucose minimal media (Min-0.9) are used as a negative control for cells expected to lack free ribosomes. At least two independent experiments were performed with similar results. **(b)** Fraction of assembled ribosomes under different growth conditions. Chemostat growth conditions include C-, N-, and P-limitations grown at 0.1 and 0.6 h^{-1}. Batch conditions include glucose minimal media (Min-0.9) and defined rich media (Rich-1.7). Mean values from three biological replicates are shown with error bars indicating the standard error of the mean.

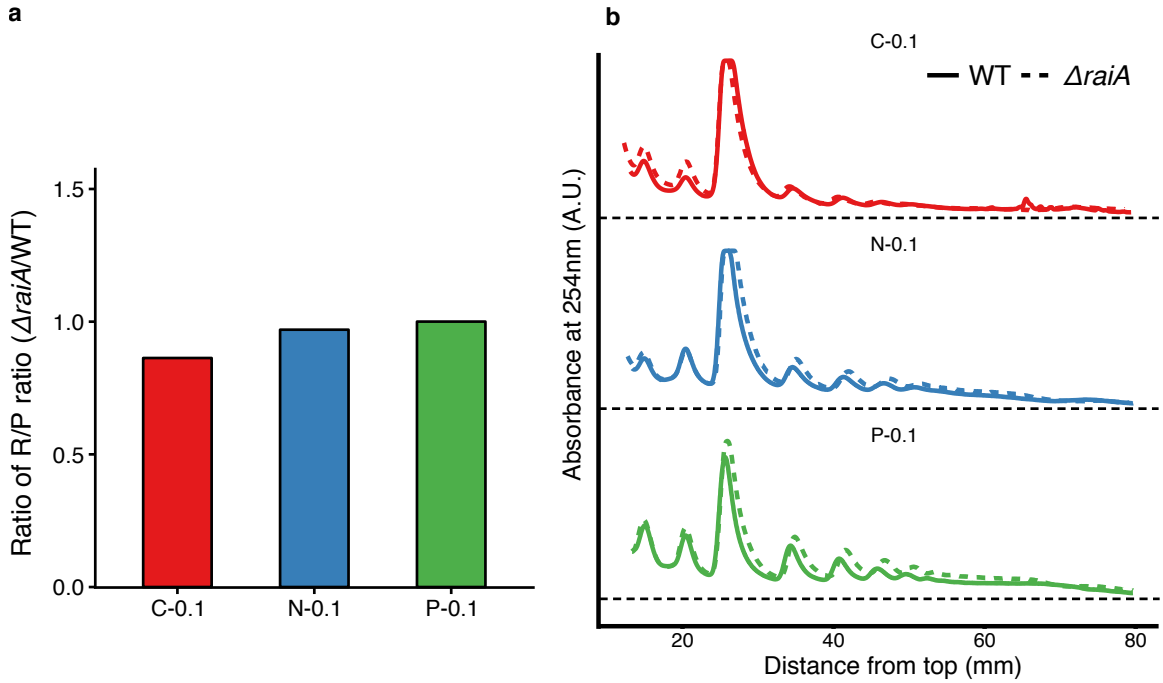

Supplementary Figure 4. (Related to Figure 1) Deletion of *raiA* does not alter ribosome dynamics. (a) The ratio of RNA-to-protein ratio of wild type and Δ*raiA* at growth rate 0.1 h^{-1} under different nutrient limitations. Each bar represents the ratio of the mean R/P ratio from three technical replicates of wild type and the mutant. **(b)** Polysome profiles of wild type and *ΔraiA* cells. Same amount of RNA from WT and *ΔraiA* was loaded for comparison. Deletion of *raiA* has no effect on the size of 70S peak. 100S peak from ribosome dimerization was not detected under any condition. The thin dashed line marks the average baseline. (*n* = 1 independent biological sample.)

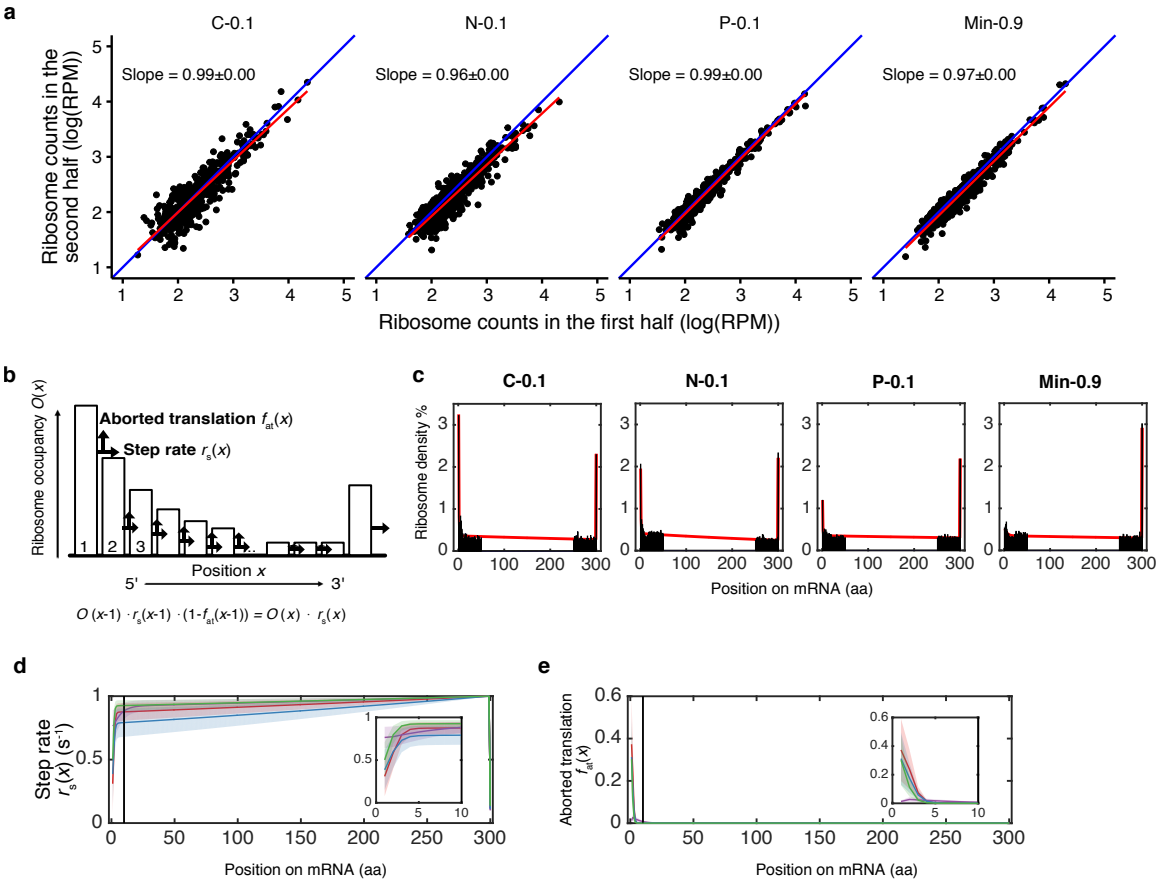

Supplementary Figure 5. (Related to Figure 2) Modeling ribosome dynamics on an mRNA with a microscopic model. (a) Comparison of ribosome density between first and second halves of genes. Scatter plot of summed RPM (reads per million) in the first and second halves of each gene. Blue line has a slope of one. Red line is the fitting result with the value of slope marked in the graph. (*n* = 1 independent biological sample.) **(b)** Illustration of the microscopic model for bound ribosome dynamics on mRNA, and the corresponding flux balance equation. **(c)** Dark bars are the normalized ribosome count in the first 50 and the last 50 codons from ribosome profiling studies. Red curves are the smoothed ribosome occupancies obtained by fitting the normalized ribosome count in the first 50 and the last 49 codons to two-term exponential functions, and copying the observed count number at the stop codon. **(d-e)** The position-dependent normalized step rate (s^{-1}) and fraction of aborted translation that best fit the smoothed ribosome occupancies in (c). Insets are magnifications for codon position 1-10.

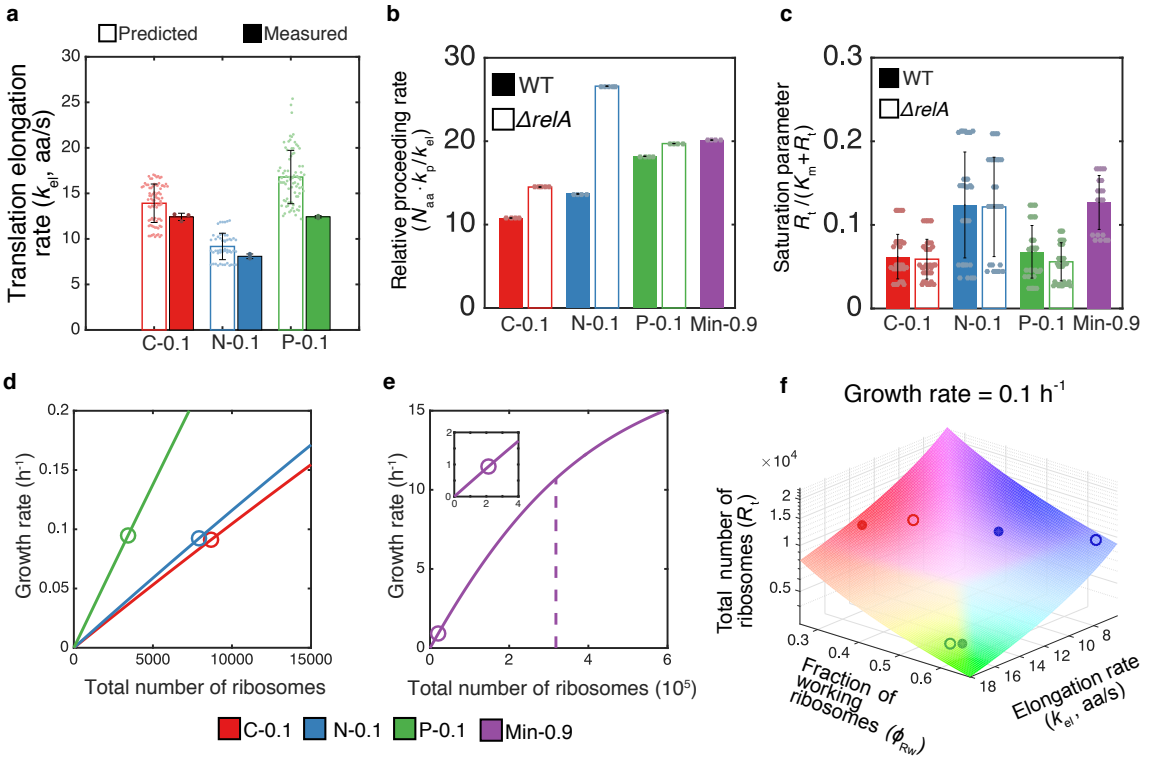

Supplementary Figure 6. (Related to Figure 2) Parameters of the macroscopic model relate translation activity and growth. **(a)** Comparison of predicted elongation rates from the macroscopic ribosome dynamics model with experimentally measured ones. The bar height represents mean values with error bars as standard deviation from all the possible combination of experimental measurements. **(b-c)** The relative proceeding rate ($N_{aa} \cdot k_p / k_{el}$) and saturation parameter ($R_t / (K_m + R_t)$) under various conditions. The bar height represents mean values with error bars as standard deviation from all the possible combination of experimental measurements. **(d-e)** Model relationships between total number of ribosomes and growth rate, while the total number of mRNAs is held constant. Dots mark the estimated values of ribosomes under each condition, and dashed line in (e) marks the half-saturation number of ribosomes under Min condition. The inset in (e) shows the region around the open circle. **(f)** The relationship between elongation rate (k_{el}), fraction of working ribosomes (ϕ_{Rw}), and total number of ribosomes (R_t) that leads to the same growth rate of 0.1 h^{-1}. Filled circles indicate the values for C-, N-, and P-limited wild type cells, and open circles indicate the corresponding values for the *ΔrelA* mutant.

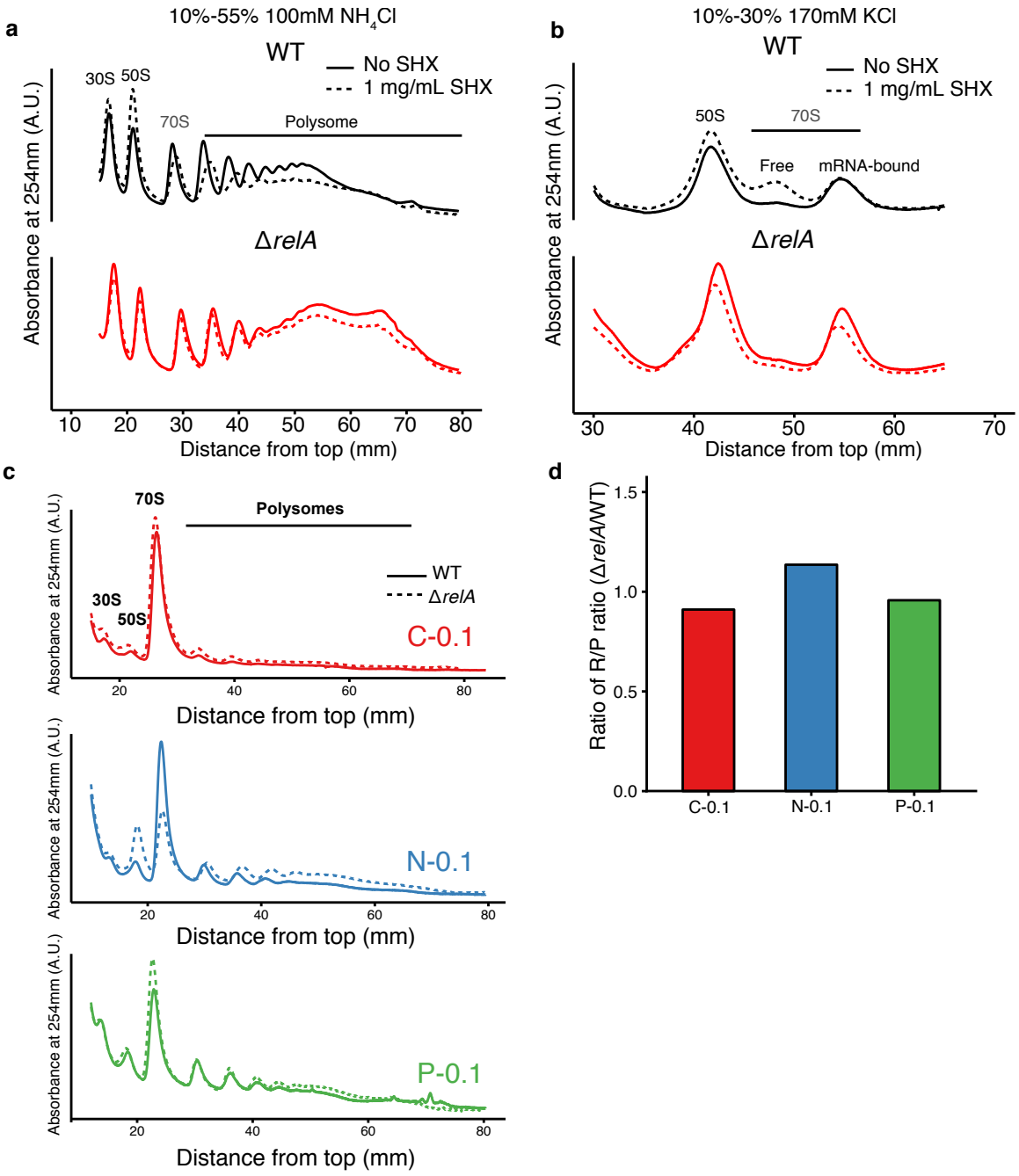

Supplementary Figure 7. (Related to Figure 3) *relA*-dependent ppGpp production leads to free ribosome accumulation under stringent response and nitrogen limitation. (a) Polysome profile of wild type and Δ*relA* cells with and without treatment of serine hydroxamate (SHX) for ten minutes. Two independent repeats were performed and one representative data is shown. **(b)** Free-ribosome profiling using 170 mM KCl to distinguish mRNA-free and mRNA-bound ribosomes. (*n* = 1 independent biological sample.) **(c)** Polysome profile of wild type and Δ*relA* cells at growth rate of 0.1 h^{-1}. Three independent repeats were performed and one representative data set is shown. **(d)** Ratios of R/P ratios of wild type and Δ*relA* at growth rate of 0.1 h^{-1}. The bar shows the ratio of the mean R/P ratio from three technical replicates of wild type and the mutant.

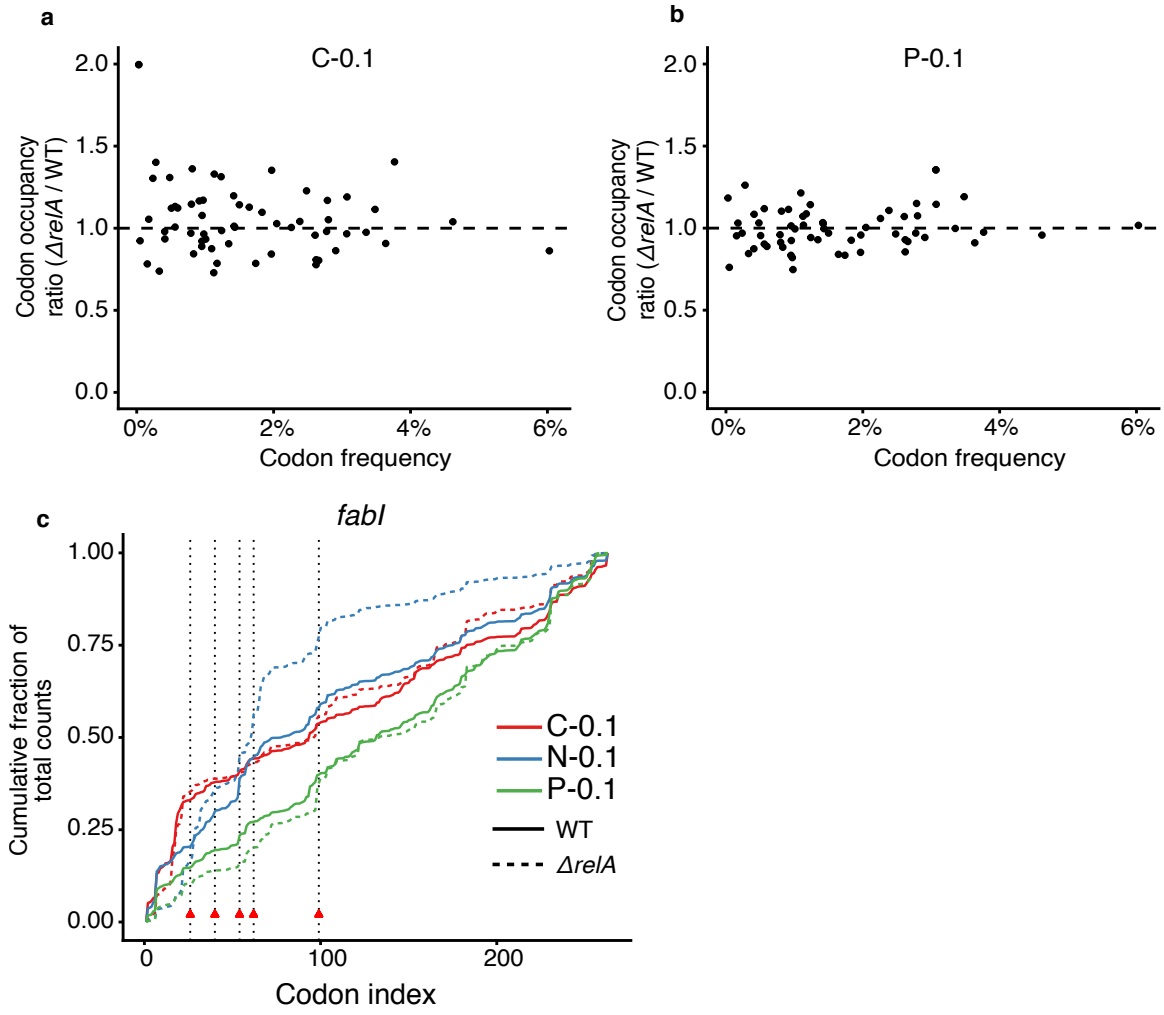

Supplementary Figure 8. (Related to Figure 3) Deletion of *relA* disrupts translation under nitrogen limitation. (a) Ratio of codon occupancy between Δ*relA* and wild type cells under carbon limitation at 0.1 h^{-1}. **(b)** Ratio of codon occupancy between Δ*relA* and wild type cells under phosphorus limitation at 0.1 h^{-1}. **(c)** Cumulative fraction of ribosome counts of *fabI* in wild type and Δ*relA* under C-, N- and P-limitations at 0.1 h^{-1}. The vertical dotted lines and red triangles mark the positions of glutamine codons.

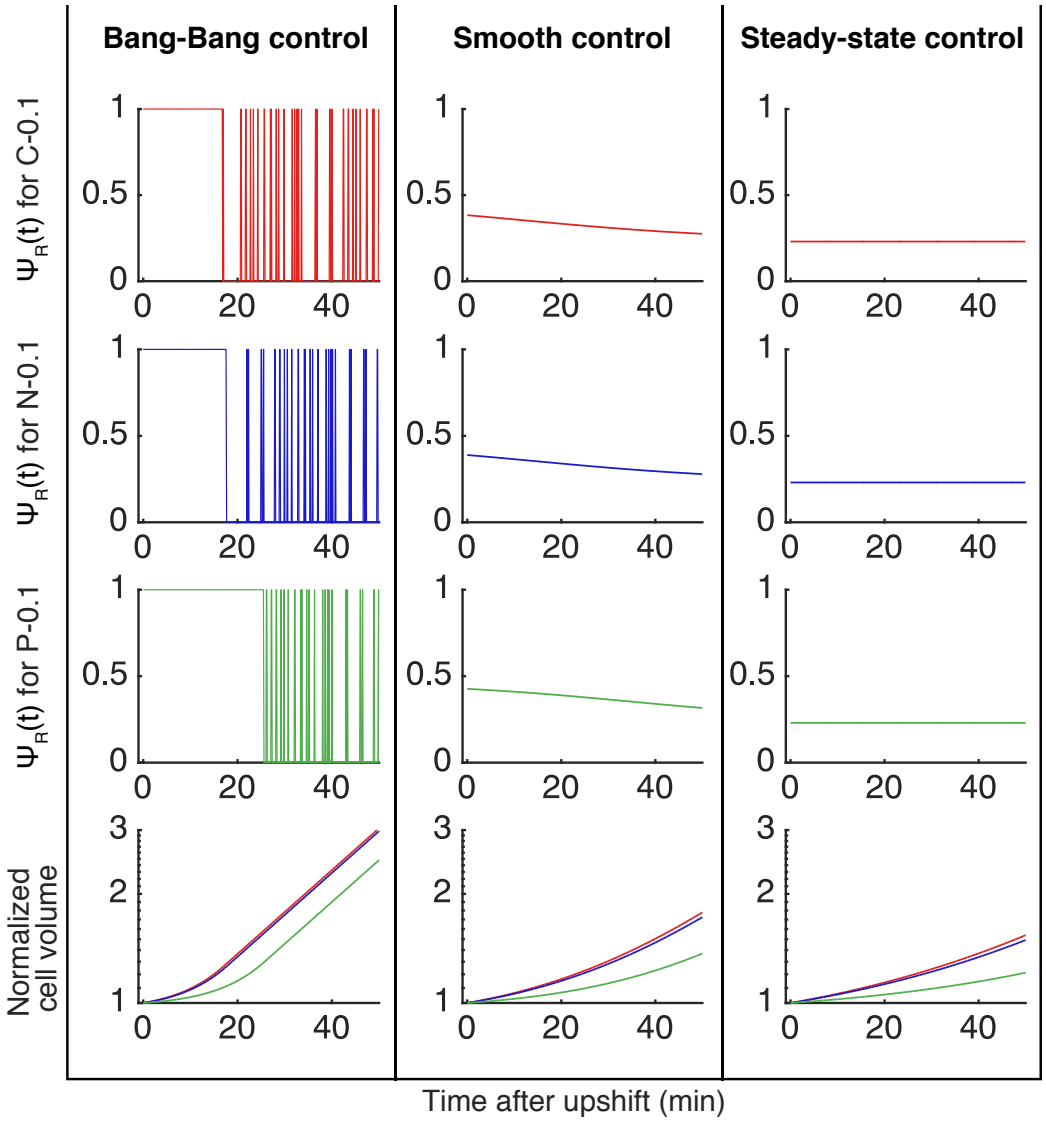

Supplementary Figure 9. (Related to Figure 4) Different allocation strategies determine growth dynamics upon modeled nutrient upshift to rich medium. After nutrient upshift to a rich condition, different regulatory strategies for $\Psi_R(t)$, the fraction of new protein synthesis allocated to ribosomal proteins (first three rows for C-, N-, and P-limitations, respectively), and their resulting post-upshift growth curves (last row).

Table S1. Definitions and values of parameters used in ribosome dynamics models.

Symbol	Definition	Value		Source
RPR	Mass ratio of total RNA to total Protein	WT C-limit	0.16	This work
		WT N-limit	0.16	
		WT P-limit	0.08	
		relA C-limit	0.16	
		relA N-limit	0.16	
		relA P-limit	0.08	
		WT Min	0.34	
		WT Rich	0.56	
μ	Steady-state growth rate (h^{-1})	WT C-limit	0.09	This work
		WT N-limit	0.09	
		WT P-limit	0.09	
		relA C-limit	0.09	
		relA N-limit	0.09	
		relA P-limit	0.09	
		Min	0.93	
		Rich	1.6	
$\emptyset_{\mathrm{Ru}}$	Fraction of ribosomes that are not bound to mRNA	WT C-limit	0.69	This work
		WT N-limit	0.49	
		WT P-limit	0.35	
		relA C-limit	0.64	
		relA N-limit	0.34	
		relA P-limit	0.37	
		WT Min	0.34	
$\emptyset_{\mathrm{Ri}}$	Fraction of ribosomes locating at the first 10 codon of mRNA, may abort translation prematurely	WT C-limit	0.03	This work
		WT N-limit	0.03	
		WT P-limit	0.03	
		relA C-limit	0.02	
		relA N-limit	0.02	
		relA P-limit	0.03	
		WT Min	0.03	
$\emptyset_{\mathrm{Rw}}$	Fraction of ribosomes locating after the first 10 codon of mRNA, contribute to the protein production in constant elongation rate	WT C-limit	0.29	This work
		WT N-limit	0.47	
		WT P-limit	0.62	
		relA C-limit	0.34	
		relA N-limit	0.64	
		relA P-limit	0.60	
		WT Min	0.63	
f_{r}	Fractional mass of rRNA among total RNA	WT C-limit	0.64	This work
		WT N-limit	0.59	
		WT P-limit	0.51	
f_{m}	Fractional mass of mRNA	0.02		[15]

	among total RNA		
V_{c}	Cell volume (m^3)	10^{-18}	[1]
C_{p}	Concentration of proteins (g/m^3)	2.4×10^{5}	[16]
m_{r}	Mass of the rRNA component in a ribosome (g)	2.8×10^{-18}	[17]
m_{nuc}	Average mass of a nucleotide in RNA in *E. coli* (g)	5.4×10^{-22}	[18]
m_{aa}	Average mass of an amino acid in *E. coli* protein (g)	1.8×10^{-22}	[19]
N_{Raa}	Number of amino acids in the ribosome	7459	[20]
N_{aa}	Average mRNA length (aa)	300	[9]
P_{m}	Total protein mass in a cell (g)	$C_{\mathrm{p}} \cdot V_{\mathrm{c}}$	
$O(x)$	Average occupancy of ribosomes at the x-th codon	Obtained by fitting the data from ribosome profiling	
$r_{\mathrm{s}}(x)$	Step rate of ribosomes from codon x to the next codon		
$f_{\mathrm{at}}(x)$	Fraction of ribosomes that abort translation during transition from codon x to the next codon		
R_{t}	Total number of ribosomes per cell	$P_{\mathrm{m}} \cdot RPR \cdot \frac{f_{\mathrm{r}}}{m_{\mathrm{r}}}$	
R_{i}	Initiating ribosomes: ribosomes located within the first 10 codons	$R_{\mathrm{t}} \cdot \emptyset_{\mathrm{Ri}}$	
R_{w}	Working ribosomes: ribosomes located within codon 11 to 301.	$R_{\mathrm{t}} \cdot \emptyset_{\mathrm{Rw}}$	
R_{u}	Unbound ribosomes, including 70S free ribosomes and subunits	$R_{\mathrm{t}} \cdot \emptyset_{\mathrm{Ru}}$	
M_{t}	Total number of mRNAs per cell	$P_{\mathrm{m}} \cdot RPR \cdot \frac{f_{\mathrm{m}}}{N_{\mathrm{aa}} \cdot m_{\mathrm{nuc}} \cdot 3}$	
M_{b}	Un-initiable mRNAs, with one ribosome bound within the first 10 codons	R_{i}	
M_{f}	Freely initiable mRNAs, with no ribosome bound within the first 10 codons	$M_{\mathrm{t}} - M_{\mathrm{b}}$	
k_{f}	Effective rate constant for unbound ribosomes and free mRNAs to initiate translation		

	(1/s)	
k_{r}	Rate constant for initiating ribosomes to abort translation (1/s)	
k_{el}	Elongation rate for working ribosomes (aa/s)	$\frac{\mu}{RPR \cdot \emptyset_{\mathrm{Rw}} \cdot 3600 \cdot m_{\mathrm{aa}} \cdot \frac{f_{\mathrm{r}}}{m_{\mathrm{r}}}}$
k_{p}	Rate constant for initiating ribosomes to transition into working ribosomes (1/s)	$\frac{k_{\mathrm{el}}}{N_{\mathrm{aa}}} \cdot \frac{\emptyset_{\mathrm{Rw}}}{\emptyset_{\mathrm{Ri}}}$
J_{P}	Total rate of protein synthesis (aa/s)	$J_{\mathrm{P}} = \mu \cdot \left(\frac{P_{\mathrm{m}}}{3600 \cdot m_{\mathrm{aa}}}\right)$ $J_{\mathrm{P}} = R_{\mathrm{w}} \cdot k_{\mathrm{el}}$
F	Relative proceeding rate	$\frac{N_{\mathrm{aa}} \cdot k_{\mathrm{p}}}{k_{\mathrm{el}}}$
S	Saturation parameter	$\frac{\frac{k_{\mathrm{r}} + k_{\mathrm{p}}}{k_{\mathrm{f}}} + R_{\mathrm{t}}}{R_{\mathrm{t}}}$
$V(t)$	Volume of the population at time t	
$g(t)$	Growth rate of the population at time t	
$\Psi_{\mathrm{R}}(t)$	Fraction of newly-synthesized proteins allocated to ribosomal proteins	
r_{t}	Concentration inside cells of total number of ribosomes	
r_{i}	Concentration inside cells of initiating ribosomes	
r_{w}	Concentration inside cells of working ribosomes	

Supplementary References

1. Bremer, H. and P.P. Dennis, *Modulation of Chemical Composition and Other Parameters of the Cell at Different Exponential Growth Rates.* EcoSal Plus, 2008. **3**(1).
2. Forchhammer, J. and L. Lindahl, *Growth rate of polypeptide chains as a function of the cell growth rate in a mutant of Escherichia coli 15.* J Mol Biol, 1971. **55**(3): p. 563-8.
3. Klumpp, S., et al., *Molecular crowding limits translation and cell growth.* Proc Natl Acad Sci U S A, 2013. **110**(42): p. 16754-9.
4. You, C., et al., *Coordination of bacterial proteome with metabolism by cyclic AMP signalling.* Nature, 2013. **500**(7462): p. 301-6.
5. Scott, M., et al., *Interdependence of cell growth and gene expression: origins and consequences.* Science, 2010. **330**(6007): p. 1099-102.
6. Norris, T.E. and A.L. Koch, *Effect of growth rate on the relative rates of synthesis of messenger, ribosomal and transfer RNA in Escherichia coli.* J Mol Biol, 1972. **64**(3): p. 633-49.
7. Dennis, P.P., *Regulation of ribosomal and transfer ribonucleic acid synthesis in Escherichia coli B-r.* J Biol Chem, 1972. **247**(9): p. 2842-5.
8. Kjeldgaard, N. and C. Kurland, *The distribution of soluble and ribosomal RNA as a function of growth rate.* Journal of molecular Biology, 1963. **6**(4): p. 341-348.
9. Milo, R. and R. Phillips, *Cell biology by the numbers*. 2016, New York, NY: Garland Science, Taylor & Francis Group. xlii, 356 pages.
10. Tuller, T., et al., *An evolutionarily conserved mechanism for controlling the efficiency of protein translation.* Cell, 2010. **141**(2): p. 344-54.
11. Subramaniam, A.R., B.M. Zid, and E.K. O'Shea, *An integrated approach reveals regulatory controls on bacterial translation elongation.* Cell, 2014. **159**(5): p. 1200-1211.
12. Stanssens, P., E. Remaut, and W. Fiers, *Inefficient translation initiation causes premature transcription termination in the lacZ gene.* Cell, 1986. **44**(5): p. 711-8.
13. Shah, P., et al., *Rate-limiting steps in yeast protein translation.* Cell, 2013. **153**(7): p. 1589-601.
14. Ingolia, N.T., et al., *Genome-Wide Analysis in Vivo of Translation with Nucleotide Resolution Using Ribosome Profiling.* Science, 2009. **324**(5924): p. 218-223.
15. Magasanik, B., *Growth of the Bacterial-Cell - Ingraham,Jl, Maaloe,O, Neidhardt,Fc.* Cell, 1983. **35**(2): p. 345-346.
16. Albe, K.R., M.H. Butler, and B.E. Wright, *Cellular concentrations of enzymes and their substrates.* J Theor Biol, 1990. **143**(2): p. 163-95.
17. Sundararaj, S., et al., *The CyberCell Database (CCDB): a comprehensive, self-updating, relational database to coordinate and facilitate in silico modeling of Escherichia coli.* Nucleic Acids Research, 2004. **32**: p. D293-D295.

18. Nierlich, D.P., *Regulation of Ribonucleic-Acid Synthesis in Growing Bacterial Cells .1. Control over Total Rate of Rna-Synthesis.* Journal of Molecular Biology, 1972. **72**(3): p. 751-764.
19. Spahr, P.F., *Amino Acid Composition of Ribosomes from Escherichia-Coli.* Journal of Molecular Biology, 1962. **4**(4): p. 395-&.
20. Wittmann, H.G., *Components of bacterial ribosomes.* Annu Rev Biochem, 1982. **51**: p. 155-83.